Superfluidity of Light and Its Breakdown in Optical Mesh Lattices

Martin Wimmer,[1] Monika Monika ,[1] Iacopo Carusotto ,[2] Ulf Peschel,[1] and Hannah M. Price [3]

[1]*Institute of Condensed Matter Theory and Optics Friedrich-Schiller-University Jena, Max-Wien-Platz 1, Jena D-07743, Germany*
[2]*INO-CNR BEC Center and Dipartimento di Fisica, Università di Trento, Povo I-38123, Italy*
[3]*School of Physics and Astronomy, University of Birmingham, Edgbaston Park Road, West Midlands B15 2TT, United Kingdom*

Hydrodynamic phenomena can be observed with light thanks to the analogy between quantum gases and nonlinear optics. In this Letter, we report an experimental study of the superfluid-like properties of light in a $(1 + 1)$-dimensional nonlinear optical mesh lattice, where the arrival time of optical pulses plays the role of a synthetic spatial dimension. A spatially narrow defect at rest is used to excite sound waves in the fluid of light and measure the sound speed. The critical velocity for superfluidity is probed by looking at the threshold in the deposited energy by a moving defect, above which the apparent superfluid behavior breaks down. Our observations establish optical mesh lattices as a promising platform to study fluids of light in novel regimes of interdisciplinary interest, including non-Hermitian and/or topological physics.

The last decades have witnessed an impressive development of new conceptual links between the apparently disconnected fields of nonlinear optics and many-body physics of quantum gases [1]. The formal analogy between the paraxial light propagation in nonlinear media and the Gross-Pitaevskii equation of dilute Bose-Einstein condensates was first noticed in the 1970s and immediately suggested the transfer of concepts such as superfluidity and quantized vortices to optical systems [2–6]. This connection was further revived with the experimental observation of Bose-Einstein condensation in exciton-polariton gases in semiconductor microcavities [7], which triggered a strong interest from both theory and experiment to address basic features of condensates such as super-fluidity, hydrodynamics, and topological excitations [8–10] in the new context of fluids of light.

In this work, we introduce a new platform for studying fluids of light by using classical light in a so-called optical mesh lattice. The idea is to encode one (or even more [11,12]) discrete synthetic spatial dimensions in the arrival time of optical pulses that propagate along coupled optical fiber loops [13–15]. This allows for the application of arbitrary dynamical potentials to the fluid of light and for the measurement of its evolution in real time with key advantages over traditional systems. In contrast to semiconductor microcavities [1], our system provides great flexibility in the design of different lattice geometries with no fabrication effort and naturally offers site-resolved access to the temporal dynamics of the fluid without the need for sophisticated ultrafast optics tools. In contrast to bulk nonlinear systems [16–18], the nonlinearity stems from the power dependent propagation constant of optical fibers and is thus fully controllable with standard opto-electronic tools. Although the potential of such optical mesh lattices for studies of linear and nonlinear optics has been demonstrated in many works on, e.g., PT-symmetric physics [12,14,15,19–21] and topological effects [22–25], here we report their first use as a platform to investigate fluids of light. In the future, it will be of great interest to further exploit the flexibility of optical mesh lattices to study fluids of light in topological and/or non-Hermitian regimes that are not straightforwardly realized in standard platforms, e.g., combining interactions with synthetic magnetic fields, topological lattices [26], and complex gain and loss distributions [27,28].

The experimental setup and the theoretical model.—In our experiments, an optical mesh lattice is realized using a time-multiplexing scheme based on two optical fiber loops of average length $\bar{L} = 4$ km, which have a small length difference $\delta L = 50$ m and which are coupled by a 50/50 beam splitter, as shown in Fig. 1(a). A light pulse injected into one loop is split by the coupler into two pulses: one circulating in the longer and one in the shorter loop. After a round-trip, the two pulses arrive back at the coupler but now with a relative time delay due to the small length difference between the loops. Each pulse is again split into two by the beam splitter, which, after many round-trips, eventually leads to the generation of a pulse train over time, as reviewed in the Supplemental Material [29].

There is a clear separation of timescales between the average round-trip time $\bar{T}$ and the relative time delay ΔT as $\bar{T} \gg \Delta T$. Thus, for not too many round-trips m ($m\Delta T < \bar{T}$) the arrival time of each pulse at the beam splitter can be unambiguously expanded as $t = m\bar{T} + n\Delta T/2$, where the integer m denotes the total number of round-trips for each pulse and the integer n counts how many more round-trips were made in the long rather than in the short loop [29]. As the light propagates, the assigned integer m keeps
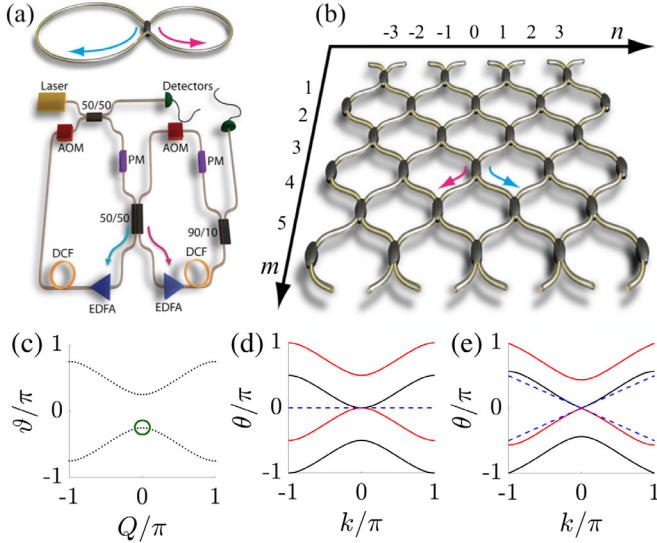
FIG. 1. (a) Optical pulses propagating in two nonlinear, coupled fiber loops of slightly different lengths, are used to explore nonlinear light evolution in the $(1+1)$D lattice, shown schematically in (b). In this mapping, the light intensity is a function of the discrete position in the lattice, n, and evolves with respect to the discrete time step, m. Completing a round-trip in the short (long) loop in the real system in (a) corresponds to traveling from northeast (northwest) to southwest (southeast) in the effective lattice in (b). Acousto-optical modulators (AOM) and erbium doped fiber amplifiers (EDFA) are used to compensate for losses. A phase modulator (PM) in each loop allows us to induce arbitrarily designed space- and time-dependent potentials. (c) The corresponding photonic bands in the linear ($\Gamma = 0$) regime. (d),(e) The Bogoliubov dispersions (2) on top of a condensate located at $Q = 0$ in the lower band [circle in (c)] for (d) linear and (e) nonlinear ($\Gamma I_0 = 0.2$) systems. The slope of the straight blue dashed line indicates the speed of sound (3). The red (black) color of each curve indicates the positive (negative) value of the band's Bogoliubov norm.

increasing to count each successive round-trip, while the integer n increases or decreases by one after each round-trip depending on which loop is traversed. The integer m is interpreted as a discrete time step, and n as a discrete position index along a "synthetic spatial dimension," leading to the effective $(1+1)$D lattice shown in Fig. 1(b) [13–15]. Even though this dynamics is intrinsically discrete in both space and time, for spatiotemporally slow fields it has an intriguing continuum limit of a Dirac model [29].

To explore nonlinear phenomena, dispersion compensating fiber (DCF) spools form part of the long and the short loops. These DCFs have a narrow core size and thus a high effective nonlinear coefficient [31] of approximately 7/km/W, leading to significant nonlinear effects in our experiment [32]. We use DCF spools with a length of approximately 4 km and employ peak powers on the order of 100 mW. To sustain such high power, erbium-doped fiber amplifiers are used to compensate for round-trip losses. As reviewed in the Supplemental Material [29],

the significant Kerr nonlinearities lead to a power-dependent phase-shift for the propagating light pulses, as captured by [19,33,34]

$$u_n^{m+1} = \frac{1}{\sqrt{2}}\left(u_{n+1}^m e^{i\Gamma|u_{n+1}^m|^2} + iv_{n+1}^m e^{i\Gamma|v_{n+1}^m|^2}\right)e^{i\varphi_n^m},$$

$$v_n^{m+1} = \frac{1}{\sqrt{2}}\left(v_{n-1}^m e^{i\Gamma|v_{v-1}^m|^2} + iu_{n-1}^m e^{i\Gamma|u_{n-1}^m|^2}\right)e^{i\phi_n^m}, \quad (1)$$

where $\Gamma > 0$ quantifies the effect of the nonlinear refractive index per round-trip, corresponding to a negative interaction energy in the quantum fluids language. Here, u_n^m and v_n^m denote the amplitudes of the pulses incident on the beam splitter from the short and long loops, respectively. The time-dependent linear phase shifts φ_n^m and ϕ_n^m are externally controlled through phase modulators inserted in each loop, and can be used, for example, to imprint defects or trapping potentials on the fluid of light.

As the equations are periodic in both position n and time step m, they can be solved in the linear regime ($\Gamma = 0$) using a Floquet-Bloch ansatz [15,35]. This gives two bands, which are 2π periodic in both the propagation constant or "quasienergy" ϑ and the "Bloch momentum" Q along the 1D lattice, with a dispersion relation $\cos\vartheta = \cos Q/\sqrt{2}$ as shown in Fig. 1.

Sound excitations.—The linear dynamics of small excitations, δu_n^m and δv_n^m, on top of a strong field, u_n^m and v_n^m, can be described within the Bogoliubov theory of dilute Bose-Einstein condensates [36,37]. For simplicity, we consider the case where the fluid of light is spatially uniform with the same amplitude $\sqrt{I_0}$ in both loops and is initially at rest in the m, n coordinate system. This corresponds to a condensate of density I_0 in the lower band eigenstate at $Q = 0$ marked by a circle in Fig. 1(c). Analytical manipulations lead to the Bogoliubov dispersion relation [35,38]

$$\cos\theta = \frac{1}{2}\Gamma I_0 \cos k + \frac{1}{2}\cos k$$
$$\pm \frac{1}{2}\sqrt{(\Gamma^2 I_0^2 + 2\Gamma I_0 + 1)\cos^2 k + 2\sin^2 k - 4\Gamma I_0}, \quad (2)$$

where θ and k are, respectively, the quasienergy and the Bloch momentum (both of period 2π) of the small perturbation. This dispersion has two positive and two negative branches as shown in Fig. 1(d) for the linear ($\Gamma I_0 = 0$) and (e) a weakly nonlinear ($\Gamma I_0 = 0.2$) case.

At small momenta, this Bogoliubov dispersion can be expanded as $\theta(k) = \tilde{v}_S|k| + \mathcal{O}(|k|^3)$, indicating that the long wavelength excitations are phononlike, with a speed of sound

$$\tilde{v}_S = \sqrt{\Gamma I_0/(1 - \Gamma I_0)} \quad (3)$$

that grows for increasing nonlinearity faster than the usual square-root dependence of a simple Gross-Pitaevskii

superfluid [36]. Note that the positive sign of the nonlinear refractive index in the considered DCFs forced us to work with a negative-mass photonic band [i.e., the top of the lower band in Fig. 1(c)] to avoid dynamical modulational instabilities. An upper bound to the sound speed is imposed by further dynamical instabilities of different nature that are found for $\Gamma I_0 > 0.5$ [35].

Probing the speed of sound.—As a first step, we investigate the propagation of spatially narrow excitation pulses on top of a wide field. We initially prepare the optical field at rest with a wide Gaussian profile corresponding to an equal amplitude in each loop at $m = 0$: $u_n^0 = v_n^0 = \sqrt{I_0}e^{-n^2/\sigma_g^2}$, where $\sigma_g \simeq 8$. Changing the input pulse power between experimental runs allows us to study the effect of nonlinearity in detail. Note that according to the notation introduced in (1) only every second lattice site is occupied as the effective lattice has diamondlike connectivity [Fig. 1(b)].

To perturb this wide fluid of light, we rapidly turn on and off a strong and spatially localized defect potential φ_d, imprinted via the time-dependent phase shifts in (1) as

$$\varphi_n^m = \phi_n^m = \Phi_d \equiv \varphi_d e^{-(n-n_d)^2/\sigma_n^2} e^{-(m-m_d)^2/\sigma_m^2}, \quad (4)$$

where φ_d is the defect amplitude, σ_n (σ_m) is related to the defect width with respect to position (time) and n_d (m_d) marks the position (time) of the defect. We choose $\varphi_d = \pi/10$ to ensure a sufficient contrast between the perturbed and unperturbed signal, and $\sigma_n = 1$ and $\sigma_m = 2$ so that the defect is short enough to excite low-momentum perturbations. The defect peak amplitude is at $m_d = 20$ and $n_d = 0$, and the propagation is observed over a long time until $m_{\max} = 110$.

The propagation dynamics of the emitted waves is measured by the differential intensity $\Delta I = I_{\text{pert}} - I_{\text{unpert}}$, where $I_{\text{pert}} = |u_n^m|^2 + |v_n^m|^2$ in the perturbed experiment, and similarly for I_{unpert} in the unperturbed case. This is plotted in Fig. 2(a) for two different values of the effective nonlinearity: $\Gamma_{\text{eff}} \propto \Gamma I_0$, where I_0 is the initial light intensity that we can control. As can be seen, the defect emits a train of excitations which spread out over time [39]. We expect the slowest strong emission to be that associated with sound waves, and so we fit $\Delta I(n)$ at each time step to extract the position of the minima [29]. The corresponding average speed, v_M, of the minima at late times is plotted in Fig. 2(b).

In order to extract the value of the speed of sound, we need to take into account the fact that the underlying fluid of light is also itself expanding during the experiment, dragging all excitations along with it. Hence, we numerically estimate a local expansion speed by applying a discretized continuity equation to the unperturbed evolution [29]. The corresponding average expansion speed, v_E, at the position of the minima at late times is plotted in Fig. 2(b). By comparing these speeds, we finally obtain the
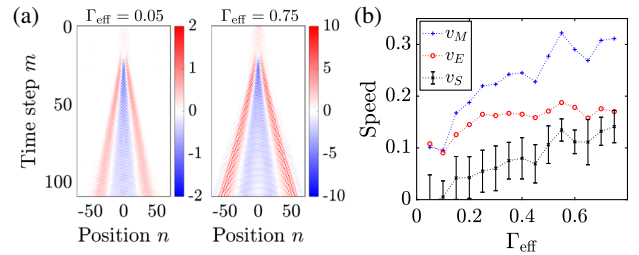

FIG. 2. (a) Experimentally observed propagation of perturbations induced by imposing a short and localized phase defect onto a Gaussian fluid of light for two different values of the effective initial nonlinearity, $\Gamma_{\text{eff}} \propto \Gamma I_0$. The colorscale represents the differential intensity, ΔI, between the perturbed and unperturbed experiments. All parameters are stated in the main text. (b) The estimated speed of sound $v_S = v_M - v_E$ grows from around zero with increasing nonlinearity. Also plotted are v_M, the average speed of the innermost minima at late times obtained by fitting the results in (a), and v_E, the average expansion speed of the unperturbed fluid of light at the minima positions, from which the sound speed was extracted. For clarity, error bars for v_M and v_E are shown in the Supplemental Material [29]. Lines are included as a guide to the eye.

estimate for the speed of sound $v_S = v_M - v_E$ plotted in Fig. 2(b). Due to experimental uncertainties, we did not fit our data to the analytical sound speed (3), but our results clearly show the expected qualitative trend as we measure v_S as being close to zero at low power, and then rising with increasing nonlinearity. One may argue that the local light intensity and hence the local nonlinearity and speed of sound can vary over time. However, as we show in the Supplemental Material [29], the local light intensity remains relatively stable because the amplifiers largely compensate for any intensity drops. The alternative way of plotting the data as a function of the averaged unperturbed local intensity at the position of the minimum exhibits the same qualitative features as Fig. 2(b) [29].

Friction on moving defect.—A key advantage of the nonlinear optical mesh lattice is that we can probe in the same setup the response to defects which are moving at arbitrary speeds along arbitrary trajectories. One definition of superfluidity [40] is the existence of a nonzero critical velocity below which a weak, uniformly moving defect will not excite permanent waves in the fluid. This critical velocity can be predicted by means of the so-called Landau criterion, and for a Gross-Pitaevskii superfluid corresponds to the speed of sound [36].

The situation is slightly more subtle in a lattice geometry, for which the Landau criterion predicts a vanishing critical velocity, as the k periodicity of the Bogoliubov dispersion allows any moving defect to emit excitations at larger momentum. In this sense, a lattice system can never truly be a superfluid, but in practice the excitation efficiency for such "Umklapp waves" is negligibly small [35]. On this basis, we restrict our attention to low-transferred-momentum
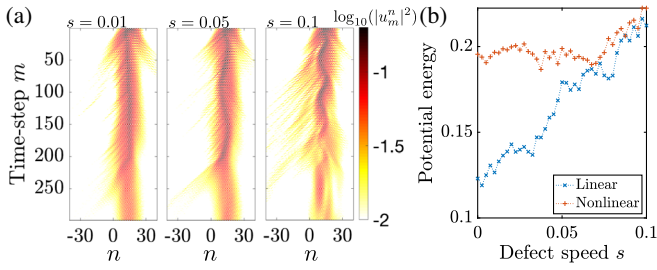
FIG. 3. (a) Spatiotemporal plot of the measured intensity in the short loop for a trapped nonlinear fluid of light ($\Gamma I \approx 0.5$ in the center of the trap) excited by a sinusoidally moving defect at various speeds s, applied to the optical field from $m = 0$ to $m = 200$. Defect and trap parameters are as given in the main text. (b) Late-time average of the potential energy (5) for experiments in the linear and nonlinear regime [nonlinear regime: power levels as in (a), linear regime: power levels 1/5 of (a)]. In the linear regime, we observe that the potential energy increases steadily with the defect speeds, while in the nonlinear regime, it remains approximately constant for low s and shows a marked upward kink at $s \approx 0.07$.

processes with $-\pi \leq \Delta k < \pi$, for which the Landau criterion predicts a minimum defect speed below which the fluid of light should not be excited substantially; this we term "superfluidlike" behavior. Note also that, within this restricted range of excitation processes, there is often also a maximum defect speed, above which the defect is moving too fast to excite the sonic branch of Bogoliubov waves but too slow to excite the other branches, again leading to apparent low dissipation. At even higher speeds, dissipation increases again as the defect moves fast enough to excite other branches.

In analogy with previous experiments with polariton fluids in semiconductor microcavities [8–10], a natural strategy to experimentally address superfluidity in our platform would then be to look at the perturbation that is induced in the density profile by a uniformly moving defect. We also performed experiments along these lines but had to fight serious experimental obstacles resulting from the finite size of our photon fluid. Its resulting rapid expansion together with the corresponding drop of its density made it difficult to extract conclusive information from the observations (see the Supplemental Material [29]).

To overcome this difficulty, a conceptually different scheme was adopted so as to exploit the peculiarities of our platform. Instead of looking at the instantaneous density perturbation, our observable is the total energy that is deposited by the moving defect into the fluid during the whole excitation sequence. Related calorimetric schemes were used to detect superfluidity in atomic gases [41–43] but were never implemented in fluids of light, mostly because of the intrinsic dissipation of microcavity systems.

More specifically, we adopted a configuration in which the optical field is excited with a defect over many time steps and the fluid is kept in place by a confining potential. For technical reasons, the trap and defect are only applied in the short loop, i.e., $\phi_n^m = 0$. The phase shift of the short loop is the sum $\varphi_n^m = \Phi_d + \Phi_t$ of the defect contribution Φ_d given in (4) and the trap one, $\Phi_t = \varphi_t(1 - e^{-(n-n_t)^2/\sigma_t^2})$. Values $\varphi_t = \pi/10$, $\sigma_t = 8$ and $n_t = 14$ of, respectively, the height, offset, and half-width of the trap are chosen in order to minimize residual motion of the trapped beam, which is initialized with the Gaussian profile detailed above. The defect is kept in the central trapped region and is moved in space along the sinusoidal trajectory defined by $n_d(m) = 4\sin(sm)$, and has $\sigma_n = 1$ and $\varphi_d = -\pi/10$. Rather than slowly switching on and off, the defect is applied with a constant amplitude from $m = 0$ until $m = 200$ so as to excite the fluid of light in a more significant way.

Excitation of the optical field by the defect is investigated looking at the spatiotemporal intensity distribution shown in Fig. 3. For all velocities, light has to adapt to the constantly changing defect potential and some light ejection can be clearly observed as light bursts propagating away from the central trapped region. But, most importantly for our superfluidity purposes, for low values of the peak defect velocity ($s = 0.01$ and $s = 0.05$) the field quickly returns to an almost quiet state once the defect has disappeared. Only a faster moving defect can efficiently transfer energy to the fluid and thus permanently change its state. This heating effect is visible for $s = 0.1$ with persistent oscillations and is a clear evidence that the defect speed was large enough for superfluidity to break down.

To make this analysis more quantitative and highlight the crucial role of superfluidity over other emission processes due to the noninertial motion of the defect [44], we estimated the deposited energy by measuring the average potential energy at late times:

$$\langle E_{\text{pot}} \rangle = \frac{1}{j+1} \sum_{m=m_{\text{max}}-j}^{m_{\text{max}}} \frac{\sum_n |u_n^m|^2 \Phi_t}{\sum_n |u_n^m|^2}, \qquad (5)$$

where j corresponds to the number of time steps after the defect is switched off; here $j = 100$. This quantity is plotted in Fig. 3(b) for experiments in the two cases of the linear and the nonlinear regime. In the linear case, we observe that the potential energy steadily increases with the defect speed. In the nonlinear regime, we see that the potential energy starts at a higher level, caused by the repelling nonlinear interaction that pushes the field up the walls of the trap and remains approximately constant for low defect speeds. A sudden threshold is visible for speeds around $s = 0.07$, after which the potential energy begins to significantly increase. This behavior can be reproduced numerically [29] and confirms the presence of an effective threshold speed, above which superfluidity breaks down and friction becomes important.

Conclusions.—In this Letter we have reported an experimental study of superfluid light in a one-dimensional optical mesh lattice where the arrival time of pulses plays the role of a synthetic spatial dimension. The unique spatiotemporal access to the field dynamics offered by our experimental setup was instrumental to perform the first direct measurement of the speed of sound in a fluid of light. The conservative dynamics of our fluid of light then allowed for a quantitative measurement of the friction force felt by a moving defect and of the consequent heating effect, providing unambiguous signature of superfluidity. Taking advantage of the flexibility of the setup in designing different geometries, ongoing work is extending the investigation to fluids of light in lattices with nontrivial geometrical [45] and topological properties [24,25] in two [12] or even higher $d > 3$ dimensions [26,46]. From a more applicative perspective, the nonlinear optical mesh platform opens exciting new avenues to exploit the interplay of interference and nonlinear optical processes for manipulations of the quantum states of optical pulses in fibers [47–49].

[1] I. Carusotto and C. Ciuti, Rev. Mod. Phys. **85**, 299 (2013).

[2] Y. Pomeau and S. Rica, C. R. Acad. Sci. Sér. 2 **317**, 1287 (1993), http://sergiorica.com/Site/Publications_files/1993cCRAS317(diffr).pdf.

[3] F. T. Arecchi, G. Giacomelli, P. L. Ramazza, and S. Residori, Phys. Rev. Lett. **67**, 3749 (1991).

[4] G. A. Swartzlander and C. T. Law, Phys. Rev. Lett. **69**, 2503 (1992).

[5] T. Frisch, Y. Pomeau, and S. Rica, Phys. Rev. Lett. **69**, 1644 (1992).

[6] K. Staliunas and V. J. S. Morcillo, *Transverse Patterns in Nonlinear Optical Resonators* (Springer, New York, 2003).

[7] J. Kasprzak, M. Richard, S. Kundermann, A. Baas, P. Jeambrun, J. Keeling, F. Marchetti, M. Szymańska, R. André, J. Staehli *et al.*, Nature (London) **443**, 409 (2006).

[8] A. Amo, J. Lefrere, S. Pigeon, C. Adrados, C. Ciuti, I. Carusotto, R. Houdre, E. Giacobino, and A. Bramati, Nat. Phys. **5**, 805 (2009).

[9] A. Amo, S. Pigeon, D. Sanvitto, V. G. Sala, R. Hivet, I. Carusotto, F. Pisanello, G. Lemnager, R. Houdr, E. Giacobino, C. Ciuti, and A. Bramati, Science **332**, 1167 (2011).

[10] G. Nardin, G. Grosso, Y. Leger, B. Pietka, F. Morier-Genoud, and B. Deveaud-Pledran, Nat. Phys. **7**, 635 (2011).

[11] A. Schreiber, A. Gbris, P. P. Rohde, K. Laiho, M. Štefaňák, V. Potocek, C. Hamilton, I. Jex, and C. Silberhorn, Science **336**, 55 (2012).

[12] A. L. M. Muniz, M. Wimmer, A. Bisianov, U. Peschel, R. Morandotti, P. S. Jung, and D. N. Christodoulides, Phys. Rev. Lett. **123**, 253903 (2019).

[13] A. Schreiber, K. N. Cassemiro, V. Potoček, A. Gábris, P. J. Mosley, E. Andersson, I. Jex, and C. Silberhorn, Phys. Rev. Lett. **104**, 050502 (2010).

[14] A. Regensburger, C. Bersch, M.-A. Miri, G. Onishchukov, D. N. Christodoulides, and U. Peschel, Nature (London) **488**, 167 (2012).

[15] M.-A. Miri, A. Regensburger, U. Peschel, and D. N. Christodoulides, Phys. Rev. A **86**, 023807 (2012).

[16] D. Vocke, T. Roger, F. Marino, E. M. Wright, I. Carusotto, M. Clerici, and D. Faccio, Optica **2**, 484 (2015).

[17] Q. Fontaine, T. Bienaimé, S. Pigeon, E. Giacobino, A. Bramati, and Q. Glorieux, Phys. Rev. Lett. **121**, 183604 (2018).

[18] C. Michel, O. Boughdad, M. Albert, P.-É. Larré, and M. Bellec, Nat. Commun. **9**, 2108 (2018).

[19] M. Wimmer, A. Regensburger, C. Bersch, M.-A. Miri, S. Batz, G. Onishchukov, D. N. Christodoulides, and U. Peschel, Nat. Phys. **9**, 780 (2013).

[20] M. Wimmer, M.-A. Miri, D. Christodoulides, and U. Peschel, Sci. Rep. **5**, 17760 (2015).

[21] M. Wimmer, A. Regensburger, M.-A. Miri, C. Bersch, D. N. Christodoulides, and U. Peschel, Nat. Commun. **6**, 7782 (2015).

[22] C. Chen, X. Ding, J. Qin, Y. He, Y.-H. Luo, M.-C. Chen, C. Liu, X.-L. Wang, W.-J. Zhang, H. Li, L.-X. You, Z. Wang, D.-W. Wang, B. C. Sanders, C.-Y. Lu, and J.-W. Pan, Phys. Rev. Lett. **121**, 100502 (2018).

[23] H. Chalabi, S. Barik, S. Mittal, T. E. Murphy, M. Hafezi, and E. Waks, Phys. Rev. Lett. **123**, 150503 (2019).

[24] A. Bisianov, M. Wimmer, U. Peschel, and O. A. Egorov, Phys. Rev. A **100**, 063830 (2019).

[25] S. Weidemann, M. Kremer, T. Helbig, T. Hofmann, A. Stegmaier, M. Greiter, R. Thomale, and A. Szameit, Science **368**, 311 (2020).

[26] T. Ozawa, H. M. Price, A. Amo, N. Goldman, M. Hafezi, L. Lu, M. C. Rechtsman, D. Schuster, J. Simon, O. Zilberberg, and I. Carusotto, Rev. Mod. Phys. **91**, 015006 (2019).

[27] Y. Ashida, Z. Gong, and M. Ueda, Adv. Phys. **69**, 249 (2020).

[28] C. Lledó, I. Carusotto, and M. H. Szymańska, arXiv:2103.07509.

[29] See the Supplemental Material at http://link.aps.org/supplemental/10.1103/PhysRevLett.127.163901 for additional results and background information, which includes Ref. [30].

[30] N. Goldman and J. Dalibard, Phys. Rev. X **4**, 031027 (2014).

[31] L. Grüner-Nielsen, M. Wandel, P. Kristensen, C. Jorgensen, L. V. Jorgensen, B. Edvold, B. Pálsdóttir, and D. Jakobsen, J. Lightwave Technol. **23**, 3566 (2005).

[32] G. Agrawal, *Nonlinear Fiber Optics*, Optics and Photonics Series (Academic Press, New York, 2013).

[33] A. Regensburger, C. Bersch, B. Hinrichs, G. Onishchukov, A. Schreiber, C. Silberhorn, and U. Peschel, Phys. Rev. Lett. **107**, 233902 (2011).

[34] C. Navarrete-Benlloch, A. Pérez, and E. Roldán, Phys. Rev. A **75**, 062333 (2007).

[35] To be published.

[36] L. Pitaevskii and S. Stringari, *Bose-Einstein Condensation and Superfluidity* (Oxford University Press, New York, 2016).

[37] Y. Castin, in *Coherent Atomic Matter Waves*, Lecture Notes of Les Houches Summer School edited by R. Kaiser, C. Westbrook, and F. David (EDP Sciences and Springer-Verlag, New York, 2001), pp. 1–136; arXiv:cond-mat/0105058.

[38] M. Wimmer, Experiments on photonic mesh lattices, Ph.D. Thesis, Friedrich-Alexander-Universitt Erlangen-Nrnberg, 2018.

[39] The small differential intensity that is visible also before the defect is applied is due to small deviations in the preparation of the initial state.

[40] A. J. Leggett, Rev. Mod. Phys. **71**, S318 (1999).

[41] C. Raman, M. Köhl, R. Onofrio, D. S. Durfee, C. E. Kuklewicz, Z. Hadzibabic, and W. Ketterle, Phys. Rev. Lett. **83**, 2502 (1999).

[42] R. Desbuquois, L. Chomaz, T. Yefsah, J. Léonard, J. Beugnon, C. Weitenberg, and J. Dalibard, Nat. Phys. **8**, 645 (2012).

[43] W. Weimer, K. Morgener, V. P. Singh, J. Siegl, K. Hueck, N. Luick, L. Mathey, and H. Moritz, Phys. Rev. Lett. **114**, 095301 (2015).

[44] V. P. Singh, W. Weimer, K. Morgener, J. Siegl, K. Hueck, N. Luick, H. Moritz, and L. Mathey, Phys. Rev. A **93**, 023634 (2016).

[45] M. Wimmer, H. M. Price, I. Carusotto, and U. Peschel, Nat. Phys. **13**, 545 (2017).

[46] T. Ozawa and H. M. Price, Nat. Rev. Phys. **1**, 349 (2019).

[47] S. Barkhofen, T. Nitsche, F. Elster, L. Lorz, A. Gábris, I. Jex, and C. Silberhorn, Phys. Rev. A **96**, 033846 (2017).

[48] Y. He, X. Ding, Z.-E. Su, H.-L. Huang, J. Qin, C. Wang, S. Unsleber, C. Chen, H. Wang, Y.-M. He, X.-L. Wang, W.-J. Zhang, S.-J. Chen, C. Schneider, M. Kamp, L.-X. You, Z. Wang, S. Höfling, C.-Y. Lu, and J.-W. Pan, Phys. Rev. Lett. **118**, 190501 (2017).

[49] M. G. Raymer and I. A. Walmsley, Phys. Scr. **95**, 064002 (2020).